**Title**
Validation of a molecular hydrogen penetration model in the electric tokamak



**Journal**
PLASMA PHYSICS AND CONTROLLED FUSION, 48(7)

**Author**
Gourdain, P A

**Publication Date**
2006-07-01

**DOI**
10.1088/0741-3335/48/7/006

Peer reviewed

# Validation of a Molecular Hydrogen Penetration Model in the Electric Tokamak

P.-A. Gourdain[a)], L. W. Schmitz

Department of Physics and Astronomy, University of California, Los Angeles CA 90095

Density profile information is invaluable to plasma experiments. In particular, the edge and mantle plasma density profile is believed to influence core plasma behavior of fusion devices such as tokamaks. In low density plasmas, light emission caused by neutral gas excitation can be used to measure the local plasma parameters. A neutral penetration model is required to evaluate plasma density from $H_\alpha$ light emission. This paper verifies that a simple three-dimensional neutral penetration model can be utilized in low density, low temperature plasmas. This model follows a three dimensional diffusion equation with directional velocity and neutrals sink. Since the $H_\alpha$ emission intensity can be linked directly to the local electron density, this model permits the reconstruction of the density profile well beyond the last closed flux surface of the plasma.

PACS: 52.25.Fi 52.25.Ya 52.55.Fa

[a] gourdain@ucla.edu

# 1 Introduction

The penetration of residual gas into tokamak plasmas is usually skin deep, especially when an H-mode is present. To illustrate this statement it is customary to express the atomic neutrals mean-free path for ionization and charge exchange by:

$$\lambda_n^H = \frac{V_n}{n_e \langle \sigma_{ion} v_e \rangle + n_i \langle \sigma_{CX} v_i \rangle}. \quad (1)$$

where $V_n$ is the speed of neutrals, $<n_e>$ is the average electron density and $<n_i>$ is the average ion density. The ionization rate coefficient $<\sigma_{ion} v_e>$ is a weak function of the electron temperature[1] $T_e$ above 30eV and peaks around 100eV at $2 \times 10^{-14}$ $m^3/s$. The charge exchange rate coefficient $<\sigma_{CX} v_i>$ is similar in magnitude. In a typical high field tokamak, $n_e$ in the mantle plasma inside the separatrix is above $1 \times 10^{19}$ particles/$m^3$ and the mean free path of "cold" (i. e. room temperature) neutrals is $\lambda^H_n < 1$ cm.

The Electric Tokamak[2] (ET) is a low field, high aspect ratio machine ($B_t = 0.25$ T, A = 5, R = 5 m, a = 1 m). Typical central parameters are $k_B T_e(0) < 250$ eV and $n_e(0) < 5 \times 10^{18}$ $m^{-3}$. Working at lower densities ($<n_e>$ stays below $3.10^{18}$ particles/$m^3$) and temperatures than other machines, the mean-free path of atomic (Franck-Condon) neutrals is around 10 cm, an order of magnitude higher than usual machines. Furthermore the average electron temperature is below 100eV (except during ICRF heating) and $H_\alpha$ light can be used to monitor neutrals behavior is the edge region. $H_\alpha$ light can also give some information on the local plasma density if the neutrals distribution is known experimentally or computed. In contrast to others tokamaks where helium puffing is mandatory to produce meaningful imaging well beyond the last closed flux surface, it is possible to look directly at hydrogen light to obtain similar results in ET. Due to the

depth of neutrals penetration, we will work in the mantle of the plasma, which is defined as the plasma region between the edge and half-radius.

ET has little recycling due to titanium gettering and the absence of porous wall materials or limiters in the vessel, as Figure 1-a shows. For this reason the study of neutral penetration needs light enhancement using gas puffing. The gas puff $H_\alpha$ imaging geometry is presented in Figure 1-b. The $H_\alpha$ emission of the gas injection is several orders of magnitude brighter than the background light. The "dark" plasma-wall interface (forming a belt-like pattern) is indicated and does not show any noticeable light.

The paper is organized as follows: Section 2 describes the physical model for light emission and neutral penetration. Section 3 focuses on the experimental results and model validation. Finally, Section 4 discusses the limits of this model and its potential for diagnostics applications.

## 2 Emission and neutral penetration model

Plasma-neutral interactions can be quite complex, mainly due to recycling and the presence of molecular and atomic hydrogen species at the plasma edge. As mentioned previously, these effects can be greatly simplified when looking at the local gas puff, providing the light emitted from the puff overwhelms the background light. In this case, only molecular hydrogen can be taken into account. It will be shown later that such a restriction is quite reasonable and does not noticeably impact on the quality of the results. After presenting the instrumentation and geometry of the experimental setup, the relation between light emission and local electron density is discussed. Then a neutral transport

model is developed and a two-dimensional plasma density distribution is derived as a function of the measured light intensity $I$.

## 2.1 Geometry and instrumentation

The molecular hydrogen gas puff for $H_\alpha$ imaging is injected through a 2-cm hole directly cut into the wall of the tokamak. Figure 1-b shows a detail view of the gas puff injection into the plasma edge. The injection is controlled by a piezo valve which regulates the gas input. This valve is located 20 cm away from the vacuum vessel wall. The whole system acts as a nozzle with a gas velocity $V_0$ along the x-axis

$$\vec{V}_0 = V_0 \vec{x} \, . \tag{2}$$

While this setup does not qualify as a typical supersonic injection[3] with an exit Mach number $M_e$ well above 1, sonic speeds are expected at the throat of the piezo valve. Using this assumption and the classical formulas for compressible flows and the gas velocity at the exit hole is given by

$$V_0 = M_{exit} \sqrt{\gamma R T_{exit}} \, . \tag{3}$$

Typical values of $M_{exit}$ are around 0.25 for this experimental setup. Figure 2 shows a schematic top view of the vacuum vessel and the relative position of camera to the gas puff orifice. The origin of the ($x$, $y$, $z$) coordinate system used in this paper is coincident with the center of the injection hole. The view angle is not normal to the injection direction and corrections will be incorporated into the coordinate system to compensate for the shallow view angle. A CCD camera (frame rate of 30 frames per second with a 5 ms integration time) is used for imaging. The next section discusses the relation between the molecular $H_\alpha$ light intensity and the local plasma density.

## 2.2 Molecular $H_\alpha$ emission model

Typical edge plasmas are characterized by many different atomic and molecular processes[4]. This is especially true in the scrape-off layer (SOL) where the interactions between neutrals and plasma are quite complex and several neutral transport codes such as DEGAS2[5] or KN1D[6] have been developed to understand such systems. In particular, they can compute the atomic and molecular neutral density, the temperature distribution and the emitted $H_\alpha$ photon rate. They have been successfully used to study edge plasma and density fluctuations[7] in tokamaks. Since we consider molecular hydrogen only in a region where there is no scrape-off layer (the plasma contacts the outboard wall where the injection hole is located) and we look at a localized volume of the plasma, it is possible to simplify the problem as follows. The hydrogen coming from the gas puff is mainly molecular, and will be supposed only molecular in the rest of this paper. The dissociation products coming from the interaction of molecular hydrogen with plasma electrons can be classified as: hydrogenic particles of mean energies between 0.3 and 7.8 eV in the ground state and first excited state (category 1), which will be considered as sinks to the molecular hydrogen density; fast excited hydrogenic particles with n = 3 (category 2), which will be considered as sinks but also as a local $H_\alpha$ light source.

The first category does not yield any $H_\alpha$ light in the volume under scrutiny (x < 50 cm from the machine wall) due to the high velocity of the dissociation products (>$7x10^3$ m/s). At the plasma densities in the mantle of ET, the ground state excitation rates to the n=3 state are below 10-20 kHz. Hence the average distance spanned before $H_\alpha$ emission is greater than 50 cm. Therefore emission from this category is outside the observation volume.

Since it takes only a few nanoseconds for the H (n=3) state to release an $H_\alpha$ photon, the second category is the only one that emits local $H_\alpha$ light. Therefore we consider here the dissociative excitation of $H_2$ into $H^*(n=3)$[8,9] and the ionization of $H_2$ into $H_2^+$ which in turns gives $H^*(n\geq 2)$[10]. The latter process is not well understood and rates are not well established. Nevertheless, recent research[11,12] suggests that the majority of atomic hydrogen produced in this process is in the n=3 state. We obtain the simple relation between $n_n$ and $I$:

$$I \propto n_n n_e \left\langle \sigma v_e \right\rangle_{ex}, \tag{4}$$

where $n_n$ is the molecular hydrogen density, $n_e$ the local electron density and $<\sigma v_e>_{ex}$ the sum of all n=3 excitation rates under consideration. To keep model simple so an analytical neutrals distribution can be found, we consider all reaction rates constant in the range of electron temperatures spanning 30 eV to 100 eV. To avoid the controversy over the excitation rate of $H_2^+$ yielding $H^*$ (n=3), we decided to use Eq. (5) in our model instead of Eq. (4).

$$I \propto n_n n_e, \tag{5}$$

Hence, no absolute intensity has been done in this paper as we are trying to develop a neutrals penetration model, discussed in the next section.

## 2.3 Molecular hydrogen diffusion model

The steady-state continuity equation for the neutrals has the general form

$$V_0 \frac{\partial n_n}{\partial x} = \frac{\partial}{\partial x}\left( D \frac{\partial n_n}{\partial x} \right) + \frac{\partial}{\partial y}\left( D \frac{\partial n_n}{\partial y} \right) + \frac{\partial}{\partial z}\left( D \frac{\partial n_n}{\partial z} \right) - k n_n \tag{6}$$

$n_n$ is the local density of neutrals. $k$ is a reaction rate which describes the sink of neutrals. $V_0$ is the initial velocity at the gas puff orifice. $D$ is a diffusion coefficient[13,14] defined by the sink and collisions of neutrals,

$$D = \frac{T_n}{m_n \left( n_e \langle \sigma v_e \rangle + n_n \langle \sigma v_n \rangle_{n-n} \right)}. \tag{7}$$

$m_n$ is the neutrals mass ($H_2$). $<\sigma v_n>_{n\text{-}n}$ is the collision rate between neutrals, at $5\text{x}10^{-15}\text{m}^3/\text{s}$[15] for ET parameters. The total reaction rate (sinking) for molecular hydrogen is $<\sigma v_e>$. It is considered constant in the mantle of ET and sums up to $5\times10^{-14}\text{m}^3/\text{s}$[16]. At the gas puff injection rate $S_{inj}$ of $10^{19}$ particles/s, we can approximate the average neutral density in the gas puff cloud to $5\times10^{16}$ particles/$\text{m}^3$, which is slightly lower than the edge plasma density. So the diffusion process is dominated by the sinking of the particles and not by the neutral-neutral collisions and we get

$$D = \frac{T_n}{m_n n_e \langle \sigma v_e \rangle}. \tag{8}$$

As discussed previously, $n_n$ describes the neutrals that do not interact with the plasma, so that $T_n$ can be considered constant and equal to $T_{exit}$. Furthermore, as Figure 1-b suggests, neutrals penetrate up to 50% of the plasma minor radius $r$. As a first approximation of the plasma density, the spatially averaged density $<n_e>_{50\%}$ will be used in the remainder of the paper. It comes from a 90 GHz microwave interferometer. It is computed assuming a parabolic density profile and calculating the average density in the outer half of the plasma (r/a > 0.5). So we obtain a Constant expression for the diffusion coefficient $D$

$$D = \frac{T_n}{k m_n} \text{ with } k = \langle n_e \rangle_{50\%} \langle \sigma v_e \rangle, \tag{9}$$

and Eq. (6) simplifies to

$$V_0 \frac{\partial n_n}{\partial x} = D \frac{\partial^2 n_n}{\partial x^2} + D \frac{\partial^2 n_n}{\partial y^2} + D \frac{\partial^2 n_n}{\partial z^2} - k n_n . \tag{10}$$

As mentioned in the last section, the gas puff originates from a 2-cm hole. The observation region is 50-cm long so the injection can be considered a point source. For these conditions, the three-dimensional neutral density distribution is given by the classical formula

$$n_n(x,y,z) = \frac{S_{inj}}{4\pi r D} \exp\left( -\frac{r\sqrt{V_0^2 + 4Dk} - V_0 x}{2D} \right) \text{ with } r = \sqrt{x^2 + y^2 + z^2} . \tag{11}$$

The imaging set-up only resolves the $x$ and $y$ direction while the light intensity is integrated along the line of sight, i.e. the $z$-direction. The high aspect ratio of ET allows the approximation of the low field side curvature by a straight line from $z = -\infty$ to $z = +\infty$. Hence the density $n_n$ ($x$,$y$) averaged over the z-direction is

$$n_n(x,y) = \frac{S_{inj}}{2\pi D} \exp\left( \frac{V_0 x}{2D} \right) \int_1^{+\infty} \frac{1}{\sqrt{u^2 - 1}} \exp\left( -A(x,y) u \right) du \tag{12}$$

where

$$u = \sqrt{1 + \frac{z^2}{x^2 + y^2}} \text{ and } A(x,y) = \frac{\sqrt{V_0^2 + 4Dk}}{2D} \sqrt{x^2 + y^2} . \tag{13}$$

The “analytical” solution of Eq. (12) is

$$n_n(x,y) = \frac{S_{inj}}{2\pi D}\exp\left(\frac{V_0 x}{2D}\right)K_0(A(x,y)) \tag{14}$$

where $K_0$ is the modified Bessel function of order 0, which can be approximated by analytic or polynomial functions[17].

### 2.4 Electron density measurement

We can now regroup both models to extract the electron density in the ET mantle plasma from the $H_\alpha$ line intensity, averaged over the *z*-direction,

$$n_e(x,y) \propto \frac{I(H_\alpha)(x,y)}{K_0(A(x,y))}\exp\left(-\frac{V_0 x}{2D}\right). \tag{15}$$

$I(H_\alpha)$ $(x,y)$ is measured directly by the camera imaging the gas puff, using an $H_\alpha$ filter. In this section we supposed the factors $D$ and $k$ are constant. Hence a simple analytic solution can be found. The experimental section of this paper demonstrates rather convincingly that these approximations yielded a computed electron density profile that matches very well the experimental data obtained via two different diagnostics. To validate this model, the next sections compare the density evaluated from the light emission with the density obtained from Langmuir probes and Thomson scattering data.

## 3 Experimental results

In the next paragraphs we focus on experimental measurements to validate the proposed model. The first paragraphs provide a succinct description of ET standard shots. A simple 1D approximation is used to explain the light intensity evolution throughout the plasma mantle. Then we verify the one-dimensional density profile obtained from light emission

against Langmuir probe data at the edge of the plasma, and Thomson scattering data further in. Finally two-dimensional density profiles are discussed.

## *3.1 ET standard shots*

ET has 3 to 5 s long shots at constant plasma current of typically $I_p \approx 50$ kA. The majority of the shots studied show good agreement between measured and calculated densities. Parts of the shots exhibiting uncontrolled position changes (due to internal disruptions) were excluded since these effects were not taken into account in our model. A comparison with other diagnostics is rather difficult during such events. To minimize this problem, only stable plasmas in contact with the outside wall of the vacuum vessel are considered here.

Figure 3 illustrates the time history of a typical shot. The plasma current is clamped to its nominal value. Despite an internal disruption at t = 2 s, the current stays constant while the plasma density decreases and then recovers. The soft x-ray (SXR) signal is indicative of the average density and temperature (weighted towards the core region). Disruptions induce a sharp drop of the SXR signal (when heat and particle losses occur). The microwave interferometer signal (Figure 3-c) shows interference fringes which correspond to an increase or decrease in the line-averaged density. The extracted plasma density is presented in Figure 3-d.

The timing of camera frames is indicated in Figure 3 by vertical dashed lines. A picture was taken every 166 ms with a 5 ms integration time. A smoothing algorithm was applied to filter out noise from the different frames. Residual background light was subtracted from the all the frames. It is important to note that this level is relatively independent of plasma density. For this particular shot, the acquisition started at t = 0.16 s and continued

until an internal plasma disruption occured, at t = 1.99 s. Figure 4 shows the spatially integrated (along *y*, *z*) light emission for different time frames. The light evolution along the x-axis clearly shows three distinctive domains. From x = 0 to x = 15 cm the light intensity increases until it reaches a maximum. The increasing plasma density causes the increase of the emission intensity. Between 15 cm and 35 cm the light slowly decreases, following an exponential decay which depends upon the plasma density. The depletion of the neutral flux determines this domain. Beyond 35 cm into the plasma, the electron/ion temperature is above 100eV and the neutral density is too low to allow useful discrimination against the background light. In this region, no information on the plasma density is available and the model cannot be verified.

### *3.2 1D spatial evolution of the $H_\alpha$ light*

Eq. (10) can be reduced to a one dimensional differential equation with only the *x* coordinate remaining. While this approximation does not permit to extract precise information from the $H_\alpha$ light, it explains the trend of the neutral light developed earlier. The solution of the diffusion equation is

$$n_n(x) = \frac{S_{inj}}{4\pi x D} \exp\left( -\frac{\sqrt{V_0^2 + 4Dk} - V_0}{2D} x \right) \tag{16}$$

and the light intensity $I(x)$ is related to the plasma density $n_e$ according to the modified equation

$$I(x) \propto n_e(x) \frac{S_{inj}}{4\pi x D} \exp\left( -\frac{\sqrt{V_0^2 + 4Dk} - V_0}{2D} x \right). \tag{17}$$

The derivative of Eq. (17) is

$$I' = \left[ \frac{n_e'}{n_e} - \left( \frac{1}{x} + \frac{\sqrt{V_0^2 + 4Dk} - V_0}{2D} \right) \right] I \,. \tag{18}$$

One should notice that the terms in Eq. (18) are positive, except *I'*. The sign of *I'* indicates which term dominates the spatial increase or decay of the intensity. As Figure 4 shows, the spatial derivative of the intensity is positive for 0 < x < 15 cm. Hence, in this region, the normalized density gradient $n_e'/n_e$ dominates and we obtain

$$\frac{I'}{I} \approx \frac{n_e'}{n_e} \text{ or } n_e \propto I \,. \tag{19}$$

In the second portion of the profile, the derivative *I'* is negative. Therefore this part is dominated by the second factor of Eq. (18). For ET parameters, the $1/x$ factor can be ignored away from the wall and in the exponential decay region is ruled by Eq. (20)

$$\frac{I'}{I} \approx -\frac{\sqrt{V_0^2 + 4Dk} - V_0}{2D} \,. \tag{20}$$

For $V_0^2 << 4Dk$, Eq. (20) becomes

$$\frac{I'}{I} \approx -k \sqrt{\frac{T_n}{m_n}}^{-1} = -\frac{1}{\lambda_n} \,, \tag{21}$$

where $\lambda_n$ is the mean free path of molecular hydrogen. This result helps to understand the different spatial domains of the light emission. After considering this simple evolution of $n_e$ and *I*, the next section tries to validate the entire model by assuming a three dimensional neutral distribution.

## *3.3 Experimental validation of the model*

To support the simple neutral diffusion model presented in this paper, we need to compare the density calculated from Eq. (15) to the density measured by other

diagnostics. A multi-tip Langmuir probe simultaneously measures the density at three radial locations $r$ = 95, 93 and 90 cm, $r$ = (1-$x$) being the minor plasma radius. The plane Langmuir probe tips are operated with a swept bias voltage and complete probe characteristics are obtained every 8 ms. The density is evaluated from the probe ion saturation current (the electron temperature is obtained simultaneously from the probe characteristics) according to[18]

$$n_p(r) = \frac{2I_{sat}(r)}{eA_p\sqrt{(kT_e + kT_i)/m_i}}. \qquad (22)$$

The ion saturation current is taken at a negative probe bias of $V_{fl}$-$kT_e/e$ where $V_{fl}$ is the probe floating potential. Data from the probe tips facing the counter-current direction were used in order to eliminate effects of non-thermal electrons on the probe characteristics. Operating at relatively low negative bias voltage ($V_{fl}$-$kT_e$)/$e$ reduces or avoids the enlargement of the effective probe area that is expected at high negative bias voltage.

If the density profile obtained from gas puff imaging is compared to the probe data, good agreement between the different data sets is found. Figure 5-a shows that the edge density profiles are consistent. The slight discrepancy for t < 0.4 s results from minor plasma movements always present at the beginning of the shots. As discussed previously, plasma motion is not taken into account in the model. Figure 5-b shows the time evolution of the density at $r$ = 70 and 75 cm for both Thomson scattering data and reconstructed density profiles. The agreement between data sets is still acceptable despite some deviation from the measured density. The data corroborate qualitatively the profile evaluated from light emission. Extensive probe and Thomson scattering measurements showed that the model is reliable for radii greater than 80 cm while verifications are more difficult between $r$ =

70 and 80 cm. The major source of uncertainties comes from the inherent error in the Thomson scattering signal and the weak light emission for r > 70 cm.

The 2-D profile reconstruction cannot be as precise as the one-dimensional case due to the simultaneous exponential decay of the neutral density along the *x*- and *y*-axis. Nevertheless it is interesting to consider trends in the 2D density contours. Figure 6 shows an example of a 2D profile. It clearly reveals the equi-density contours and the gradients expected for up-down symmetric plasmas. The useful two-dimensional data is restricted to $x < 15$ cm due to rapid light decay.

In this section the validity of Eq. (15) for describing the spatial neutral density profile was demonstrated. This simple model appears correct in the mantle of the plasma. As we approach hotter and denser region, the $H_\alpha$ emission becomes weak and validation becomes difficult. The following section considers the applications and the limitations of the model.

# 4 Discussion

The previous section validated the model by comparing density reconstruction results with other density data (Langmuir probes and Thomson scattering). The next paragraphs discuss a possible expansion of the method for practical applications such as density profile diagnostic or mantle fluctuation measurements.

Figure 7 shows the time evolution of the mantle and edge density profile (70 cm < *r* < 100 cm), calculated from Eq. (15). The region between 80 and 70 cm shows density trends rather than an accurate density profile. Reliable results are obtained for r > 80 cm. This method does not perturb the plasma and the localized light signal from the gas puff provides good spatial measurement resolution. The experimental setup does not require

any complex equipment. A low speed CCD camera can yield excellent results. The acquisition frequency competes easily with present Thomson scattering lasers (repetition rate 10 to 40 Hz).

A useful and efficient diagnostic can be developed using the neutral density model presented here. The results from Figure 5-b demonstrate its usefulness at the edge of ET, where Thomson scattering cannot resolve the density profile due to low electron density and where probes measurements are not reliable due to "high" electron temperatures perturbing the probe environment. At his location (90 cm < r < 70 cm), $H_\alpha$ density imaging can replace probes. A complementary system can be devised on ET to associate core density profiles (using Thomson scattering), with profile reconstruction from $H_\alpha$ light near the edge. The scaling factor in Eq. (15) can be defined by connecting laser and $H_\alpha$ light data where they overlap.

Fundamental characteristics of ET plasmas can be elucidated using this method. ET exhibits a particle pinch in Ohmic discharges[19], leading to a 2/1 tearing mode, which triggers an internal disruption. This particle accumulation is thought to result from a negative radial electric field which forces inward ion transport. The proposed model for neutral penetration can help to determine the time evolution of density profile and compare it with density profiles from a time evolution transport code. Figure 8 shows the differences in density profile shapes which indicates confinement changes during particle accumulation.

As demonstrated by previous work[7,20], density fluctuations and turbulence can also be studied using fast imaging systems. For ET mantle plasmas, with $n_e \approx 10^{18}$ $m^{-3}$ and Te ≈ 100 eV, the radiative de-excitation rate for $H_\alpha$ emission is around 10 MHz[21]. Hence

fluctuation studies for frequencies below 1MHz are possible, competing with the frequency response of Langmuir probes. The gas puff, however, can penetrate into the plasma beyond the region that is accessible by Langmuir probes. A matrix of optical fibers with focused optics can be used to record the puff light.

Finally we focus on the error level intrinsic to the model in the 1-D case. If we introduce an error $\tilde{k}$ in $k$ then Eq. (16) gives

$$\left|\frac{\tilde{n}_n}{n_n}\right| = \left|\frac{\tilde{k}}{k}\right| \exp\left( -\frac{\sqrt{V_0^2 + 4T_n/m_n} - V_0}{2T_n/m_n} x\left|\tilde{k}\right| \right) < \left|\frac{\tilde{k}}{k}\right| \tag{23}$$

So the error on the analytical neutral density is of the order of $\tilde{k}$. The error in the neutral density is comparable to the errors of the measured averaged plasma density and the reaction rate.

# 5 Conclusion

In this paper, we demonstrated that a simple neutral transport model can yield an accurate neutral density in deep regions of the plasma. By assuming a point source for the neutrals and solving a diffusion equation with directional velocity and sinks, the three-dimensional neutral density distribution is calculated analytically. The results presented herein correlate rather well with Langmuir probes at the edge and Thomson scattering data deeper into the mantle. A dependable one-dimensional neutral density profile is found for 80 cm < $r$ < 100 cm. Results for r < 80 cm are still acceptable but the reduced $H_\alpha$ emission limits this method to radii greater than 70 cm. Furthermore one- and two-dimensional plasma density profiles can be obtained using this technique. If a

supersonice gas puff is used, plasmas of higher densities can also be imaged using this model.

This neutral penetration model can be used as a reliable diagnostic method. It can be coupled to Thomson scattering for full density profile reconstruction, enabling continuous density measurements in regions where scattered laser light is prone to unfavorable signal to noise ratio due to low electron densities. Fluctuations can also be studied deeper into the plasma, complementing edge probe measurements. Finally more accurate comparisons with transport models and time evolution codes become feasible. Such models can be integrated with imaging to deliver a simple and rapid diagnostic for complete radial density profiles in low density machines.

## Acknowledgements

This work was funded by US DOE Grant # DE-FG03-86ER53225

---

[1] R. K. Janev *et al*., Elementary Processes in Hydrogen-Helium Plasmas, Springer-Verlag, New York (1987)

[2] R.J. Taylor, J.-L. Gauvreau, M. Gilmore, P.-A. Gourdain, D.J. LaFonteese and L.W. Schmitz, Nucl. Fusion **42,** 46 (2002).

[3] J. Bucalossi *et al*., 29th EPS Conference on Plasma Phys. and Contr. Fusion Montreux, 17-21 June 2002 ECA Vol. **26B**, O-2.07 (2002)

[4] D. H. McNeill, Journ. Of Nucl. Mat., **162-164**, 476 (1989)

[5] D. P. Stotler, C. S. Pitcher, C. J. Boswell, T. K. Chung, B. LaBombard, B. Lipschultz, J. L. Terry, R. J. Kanzleiter, Jour. Nucl. Mater., **967**, 290 (2001)

[6] B. LaBombard, PSFC/RR-01-3, MIT (2001)

[7] S. J. Zweben *et al*., Nucl. Fusion **44**, 134 (2004)

[8] R. K. Janev *et al*., Elementary Processes in Hydrogen-Helium Plasmas, Springer-Verlag, New York, pp. 50-51 (1987)

[9] G. A. Khayrallah, Phys. Rev. A, **13**, 1989 (1976)

[10] R. K. Janev *et al*., Elementary Processes in Hydrogen-Helium Plasmas, Springer-Verlag, New York, pp. 62-63 (1987)

[11] W. J. van der Zande *et al*., Phys. Rev. A, **54**, 5010 (1996)

[12] S. Tanaka *et al*., Plasma Phys. Control. Fusion **42**, 1091 (2000)

[13] D. A. Knoll *et al*., Phys. Plasmas **3**, 293 (1996)

[14] J. Catto, P. Helander, J. W. Connor, R. D. Hazeltine, Phys. Plasmas **5**, 3961 (1998)

[15] P. S. Krstic, D. R. Schultz, Atomic and Plasma-Material Interaction Data for Fusion, Vol. 8, 52 I 10.5

[16] R. K. Janev *et al*., Elementary Processes in Hydrogen-Helium Plasmas, Springer-Verlag, New York, pp. 44-55 (1987)

[17] M. Abramowitz, I. A. Stegun, *Handbook of Mathematical Functions*, Dover Publications, New York, p. 379 (1972)

[18] Lothar you need to add this

[19] R. J. Taylor *et al*., Nucl. Fusion **45**, 1634 (2005)

[20] S. J. Zweben, S. S. Medley, Phys. Fluids **B1**, 2058 (1989)

[21] . C. Johnson, E. Hinnov, J. Quant. Spectrosc. Transfer. **13**, 333 (1973)

# Figures

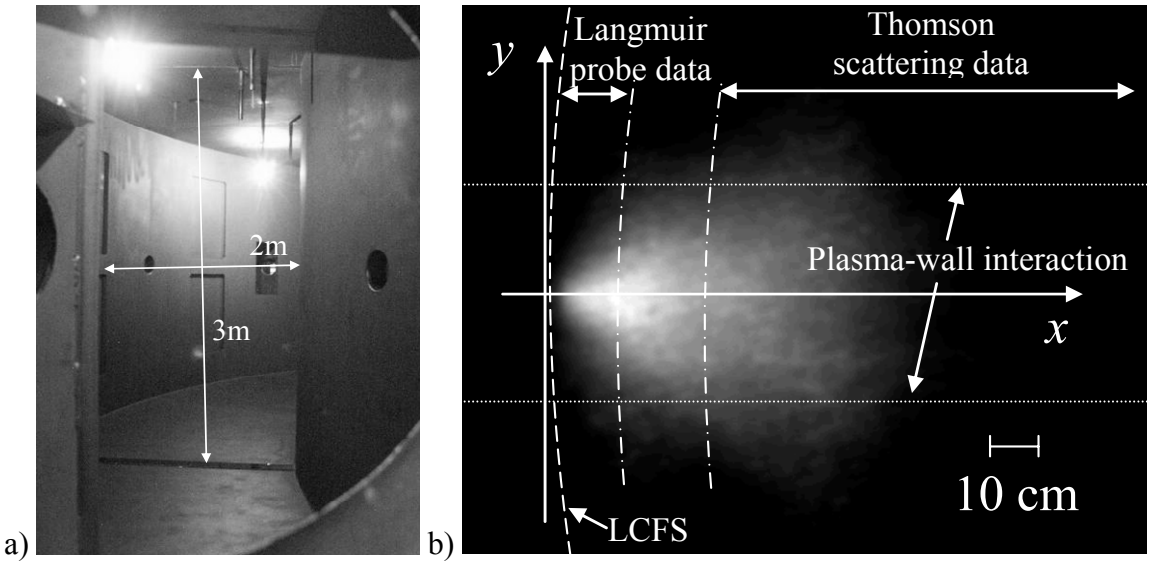


**Figure 1. a) View of the vacuum chamber of the Electric Tokamak showing bare walls and geometry during titanium gettering (bright globes near the top of the vacuum vessel); b) view of the gas puff with renormalized $H_\alpha$ light intensity. Coverage of the different profile diagnostics is indicated. $H_\alpha$ recycling light from the wall (acting as a belt limiter) and background light from the plasma are barely visible.**

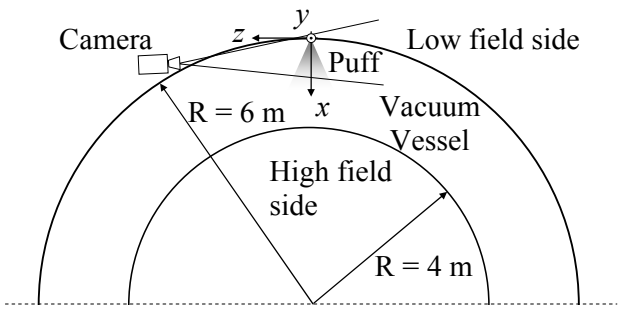


**Figure 2. Schematic view of the gas puff and camera locations in the ET experiment.**

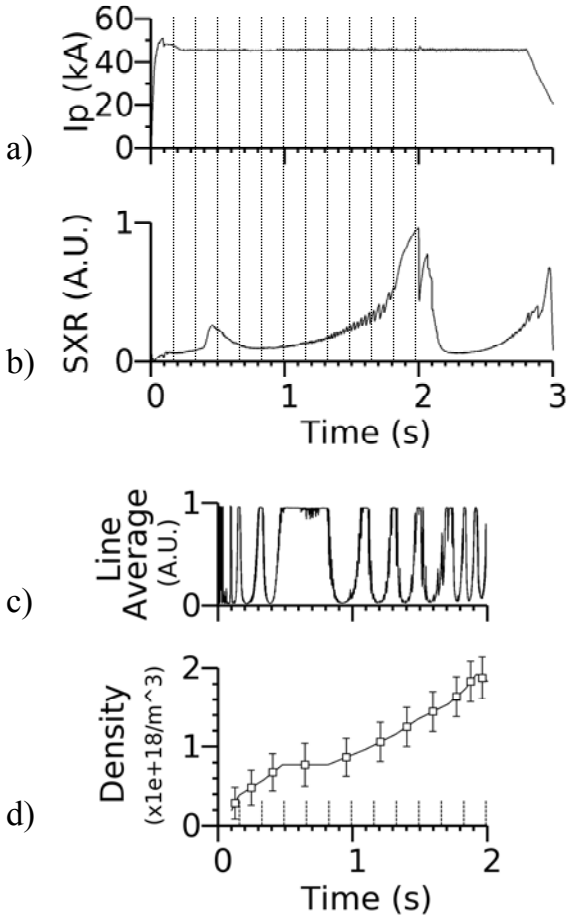


**Figure 3. a) Plasma current; b) soft x-ray signal for a typical ET shot; c) line-average density from interferometer (1 fringe corresponds to $1.7 \times 10^{17}$ particles/$m^3$) and d) $\langle n_e \rangle$ from fringe count. The dashed lines represent the times when the camera pictures were taken.**

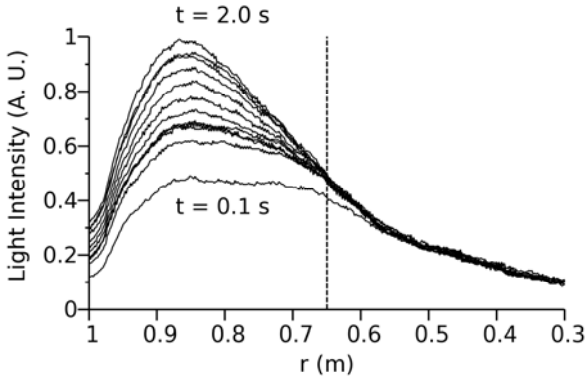


**Figure 4. $H_\alpha$ emission along the x-axis (injection direction). The light signal has been integrated along the y-axis and the background light subtracted. *r* = 1 m corresponds to the injection location. The vertical dashed line separates the region of valid data extraction (r > 0.65 m) from the area where no profile information is available (r < 0.65 m).**

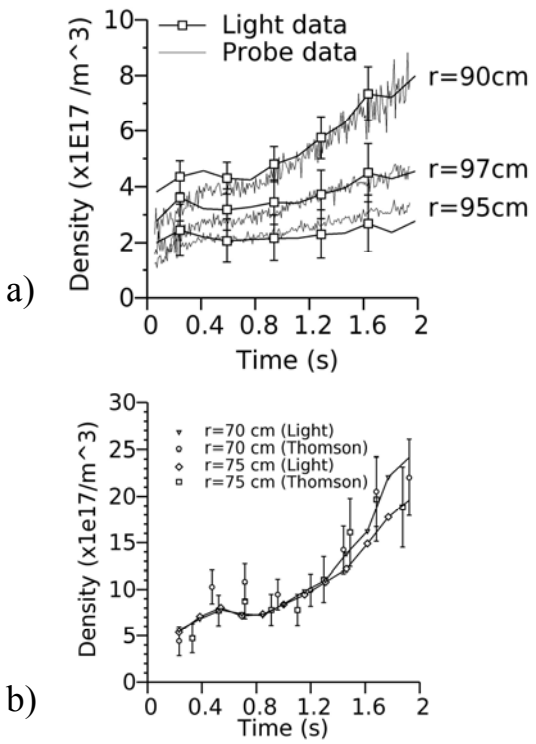


**Figure 5. a) Comparison between probe data and the reconstructed density from the $H_\alpha$ light emission for r = 95, 93 and 90 cm. The slight discrepancies between probe measurements and light data for t < 0.4 s result from minor plasma movement after start up, which our model does not take into account. Once the plasma is in a stable position, the data sets agree within the error bars of the imaging data. The edge profile scaling is also conserved; b) comparison between Thomson scattering and density profile reconstruction for r = 70 and 75 cm. The two sets of curves agree rather well. The error levels of the Thomson data and light measurements render the strict comparison between the two signals slightly difficult. Nevertheless the trends of both sets stay consistent throughout the shot.**

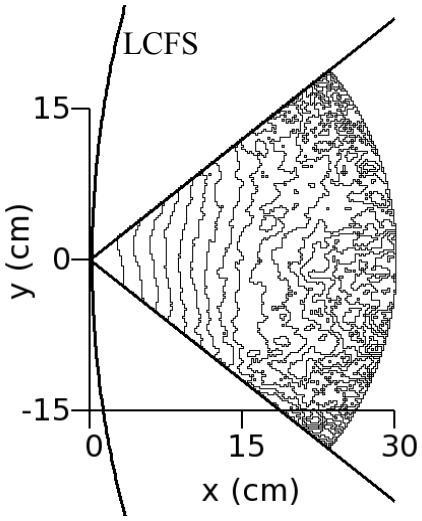


**Figure 6. Two-dimensional density profile from gas puff injection. Beyond $x$ = 15 cm ($r$ = 85 cm) the level of light is not high enough to permit extraction the 2-D information on the density profile. Only 1D reconstruction is possible beyond this limit. The solid oblic lines indicate the light detection limit of the camera. The solid arc-line corresponds to the last closed surface of the plasma. The utilization of a more sensitive camera may extend the range of the 2D reconstruction.**

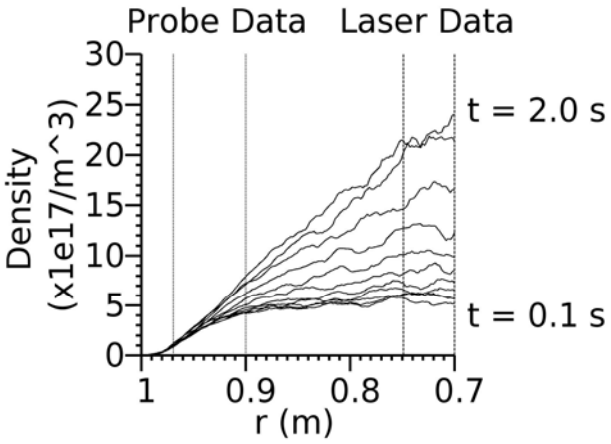


**Figure 7. 1D mantle density in particles/m$^3$ from t = 0.2 s to t = 2.0 s and spanning from r = 100 to 70 cm. The density time evolution demonstrates the possible applications of neutral imaging for density profile reconstruction. The boundaries for useful data from the different diagnostics are also shown. The last close flux surface is r = 99 cm.**

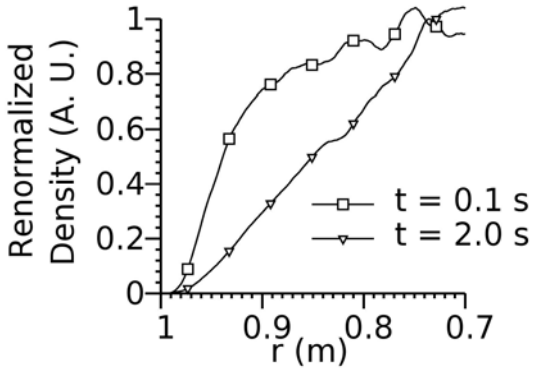


**Figure 8. Edge density profile evolution during a pinch in the Electric Tokamak. The change of curvature in the density profile is indicative of a change in confinement. The last close flux surface is r = 99 cm.**